Nucleosome-bound SOX2 and SOX11 structures elucidate pioneer factor function

https://doi.org/10.1038/s41586-020-2195-y

Received: 9 December 2019

Accepted: 18 March 2020

Published online: 22 April 2020

Check for updates

Svetlana O. Dodonova[1], Fangjie Zhu[2], Christian Dienemann[1], Jussi Taipale[2] & Patrick Cramer[1]✉

'Pioneer' transcription factors are required for stem-cell pluripotency, cell differentiation and cell reprogramming[1,2]. Pioneer factors can bind nucleosomal DNA to enable gene expression from regions of the genome with closed chromatin. SOX2 is a prominent pioneer factor that is essential for pluripotency and self-renewal of embryonic stem cells[3]. Here we report cryo-electron microscopy structures of the DNA-binding domains of SOX2 and its close homologue SOX11 bound to nucleosomes. The structures show that SOX factors can bind and locally distort DNA at superhelical location 2. The factors also facilitate detachment of terminal nucleosomal DNA from the histone octamer, which increases DNA accessibility. SOX-factor binding to the nucleosome can also lead to a repositioning of the N-terminal tail of histone H4 that includes residue lysine 16. We speculate that this repositioning is incompatible with higher-order nucleosome stacking, which involves contacts of the H4 tail with a neighbouring nucleosome. Our results indicate that pioneer transcription factors can use binding energy to initiate chromatin opening, and thereby facilitate nucleosome remodelling and subsequent transcription.

Transcription of the human genome is controlled by about 1,600 transcription factors[4]. Transcription factors recognize DNA motifs and recruit protein complexes that enable transcription initiation[5]. The binding of most transcription factors is restricted to regions of the genome that are not packaged into chromatin[6]. Some transcription factors can, however, bind to chromatin via contacts to its fundamental unit, the nucleosome[7]. These pioneer transcription factors can initiate transcription in silent chromatin regions[8], and are required for embryo development, cell differentiation and cell reprogramming[9].

SOX2 and OCT4 (also known as POU5F1) are pioneer factors that are widely used for the reprogramming of adult cells to induced pluripotent stem cells[2,10,11]. SOX2 and OCT4 can interact with nucleosomes in vitro and in vivo[12,13]. SOX2 alone can direct chromatin opening[14] and bind target DNA sites before OCT4 in vivo[10], and SOX2 binding to DNA can also follow OCT4 binding in vitro[15]. Most factors in the SOX family (hereafter, SOX factors) show pioneer factor function[7] and are essential for developmental processes[1,9]. The mutation of SOX factors can lead to severe developmental defects and cancer[16]. How pioneer transcription factors such as SOX factors bind to the nucleosome, and how they make DNA accessible for their non-pioneer partner proteins, is unknown.

To investigate this, we determined the cryo-electron microscopy (cryo-EM) structure of human SOX2 in complex with a nucleosome (Methods). We used a 147-bp nucleosomal DNA sequence (hereafter referred to as DNA-1) (Extended Data Fig. 1) that was previously selected for binding the closely related factor SOX11[7]. The DNA-binding domains (DBDs) of SOX2 and SOX11 share 83% sequence similarity (Extended Data Fig. 2), and bind the same DNA motif (TTGT)[17]. Base pairs of the TTGT core motif are specifically contacted by amino acid residues in the RPMNAFMVW signature motif of the SOX-factor HMG box[18]. SOX2 and SOX11 bind the same target sites in cells, substantially differ only in regions that flank their DBDs, and recruit different factors[19,20].

Nucleosomes containing DNA-1 bound recombinant SOX2 or SOX11 DBDs (Extended Data Fig. 3). We added the purified SOX2 DBD in excess to reconstituted nucleosomes, plunge-froze cryo-EM grids and collected cryo-EM data (Methods). A subset of 32,301 particles resulted in an approximately 5.5 Å resolution map that showed extra density on the nucleosome surface (Fig. 1, Extended Data Fig. 4, Extended Data Table 1). We fitted the map with structures of the nucleosome[21] and the SOX2 DBD[22] (Extended Data Figs. 4, 5).

The nucleosome–SOX2 structure that we obtained revealed a single copy of the SOX2 DBD bound to DNA at superhelical location (SHL) +2 (Fig. 1). The observed SOX binding involves specific interactions with the DNA motif, as confirmed by site-directed mutagenesis of involved residues in SOX11 and by mutagenesis of the DNA-1 sequence (Extended Data Figs. 3, 6). In further agreement with our structure, in vivo[23] SOX factors preferentially occupy target sites that are located near the centre of the nucleosome[24]. Although DNA-1 contains multiple SOX-binding motifs and can bind multiple copies of SOX2, nucleosomes containing DNA-1 bind only one copy of SOX2 (Extended Data Figs. 1, 3). In the context of the DNA-1 sequence, binding of the SOX DBD to other sites on the nucleosome would result in clashes with DNA and histones (Extended Data Fig. 1d).

Despite extensive efforts, the resolution of our nucleosome–SOX2 structure remained limited. We therefore determined the structure of a nucleosome bound to the DBD of SOX11 (Methods). The cryo-EM dataset contained 222,731 particles and resulted in a detailed reconstruction

[1]Department of Molecular Biology, Max Planck Institute for Biophysical Chemistry, Göttingen, Germany. [2]Department of Biochemistry, University of Cambridge, Cambridge, UK. ✉e-mail: patrick.cramer@mpibpc.mpg.de

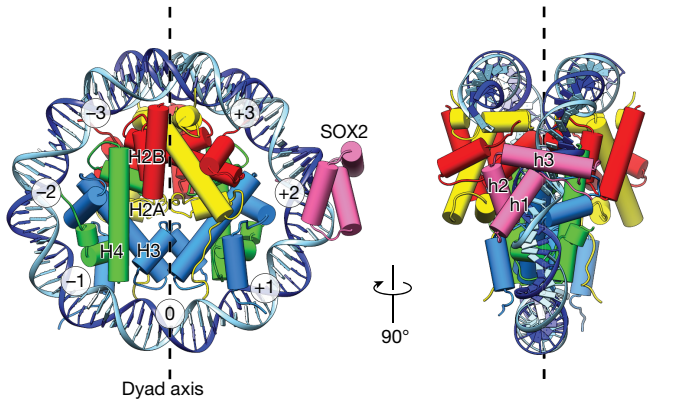

Fig. 1 | Structure of the nucleosome–SOX2 complex. Structure of the nucleosome–SOX2 complex reveals SOX2 binding at SHL +2. Top and side views are related by a 90° rotation around the dyad (dashed line). Superhelical locations −3 to +3 are labelled. SOX2 DBD is shown in pink; histones H2A, H2B, H3 and H4 are shown in yellow, red, blue and green, respectively; DNA is shown in dark and light blue. h1–h3, helices 1–3.

at 3.7 Å resolution (Extended Data Figs. 4, 5). To aid model building, we additionally determined the crystal structure of the SOX11 DBD in complex with a DNA fragment at 2.5 Å resolution (Extended Data Fig. 2c–f, Extended Data Table 2).

The structure of the nucleosome–SOX11 complex was virtually identical to that of the nucleosome–SOX2 complex (Extended Data Figs. 4g, 5). It is also a good model for nucleosome complexes with the DBDs of other members of the SOX family, which are highly conserved (Extended Data Fig. 2). For comparisons, we further determined the structure of the free nucleosome containing DNA-1 from 368,270 particles at 3.2 Å resolution (Extended Data Figs. 4, 5). This structure was highly similar to the canonical nucleosome structure (Protein Data Bank (PDB) code 6FQ5), root mean square deviation (r.m.s.d.) (P) = 1.0 Å).

Comparison of the nucleosome–SOX11 structure with the free nucleosome structure shows that SOX11 binding leads to strong local DNA distortions at SHL +2 (Fig. 2) (local r.m.s.d. (P) = 3.9 Å; calculated for 12 bp of DNA). SOX11 widens the DNA minor groove by 7 Å and pulls the DNA away from the histone octamer by 3–4 Å (coordinate error of approximately 1 Å), which increases DNA bending (Fig. 2). These DNA distortions are induced by SOX11 binding, and are also observed in our SOX11–DNA crystal structure (r.m.s.d. (P) = 1.4 Å, for 12 bp of DNA). Thus, the SOX factor uses binding energy to distort DNA locally, despite competing histone–DNA interactions.

In both nucleosome–SOX-factor structures, approximately 2.5 turns of both DNA termini are detached from the histone octamer and not visible in the cryo-EM densities (Fig. 3, Extended Data Fig. 5). This is consistent with the observation that several SOX factors facilitate DNA unwrapping from the nucleosome[7], and with the known high dynamics of the terminal DNA[25,26]. A DNA cleavage assay supports the increase in accessibility of the terminal nucleosomal DNA in the presence of SOX11 (Extended Data Fig. 7). Comparison with the free nucleosome structure indicates that terminal DNA at SHL −7, SHL −6 and SHL −5 is detached from the octamer because of a clash with helix 2 of the SOX factor (Fig. 3c, Supplementary Video 1). Thus SOX factor binding to the nucleosome facilitates DNA detachment and increases accessibility of terminal DNA.

Our cryo-EM data also suggest the dynamics that underlie nucleosome invasion by SOX factors. A set of particles from a separate dataset (151-bp DNA-1) (Methods) resulted in an alternative nucleosome–SOX11 structure in which the terminal DNA near SOX11 remained associated with the histone octamer (hereafter, nucleosome–SOX11*) (Fig. 3, Extended Data Figs. 4, 5). Thus, SOX factors may initially bind to their target site without detaching the second DNA gyre. Movement of the DNA-bound SOX factor to the position observed in the nucleosome–SOX11 structure would then lead to a clash that is resolved by terminal DNA detachment. This resulted in a model of nucleosome invasion and DNA unwrapping by SOX-factor binding (Fig. 3, Supplementary Video 1). The proposed mechanism differs from that used by the yeast pioneer factor Reb1, which binds and traps terminal DNA[27].

In our nucleosome–SOX factor structures, terminal DNA is detached on both sides of the nucleosome, which suggests an additional allosteric effect of the SOX factor on nucleosome stability. Detachment of terminal DNA on the other side of the nucleosome may be stabilized by binding of a second copy of the SOX factor at SHL −2, which we observed in a subpopulation of our cryo-EM particles (Extended Data Figs. 4, 5e). In this nucleosome–$SOX11_2$ structure, the orientation of SOX-factor binding is determined by the asymmetric DNA motifs at both SHL +2 and SHL −2, with the latter apparently having lower affinity (Extended Data Figs. 3, 6). We speculate that SOX factors may also bind to multiple sites of a nucleosome in vivo. For example, a well-studied SOX2-binding genomic location (LIN28) contains two canonical SOX2 DNA motifs within a nucleosome and shows a broad peak of SOX2 occupancy[12].

The nucleosome–$SOX11_2$ structure shows that SOX11 binding at SHL −2 is incompatible with binding of terminal DNA at SHL +7, SHL +6 and SHL +5, although the predicted clash at this location is with helix 3 and both termini of the SOX-factor DBD. DNA detachment is also observed with the use of Förster resonance energy transfer experiments when SOX11 is present at high concentrations (Extended Data Fig. 7). Thus, SOX factors can induce detachment of both DNA ends and can bind to both sides of the nucleosome (Fig. 3, Supplementary Video 1). These observations agree with the recently described strong preference for SOX2 binding at approximately ±25 bp around

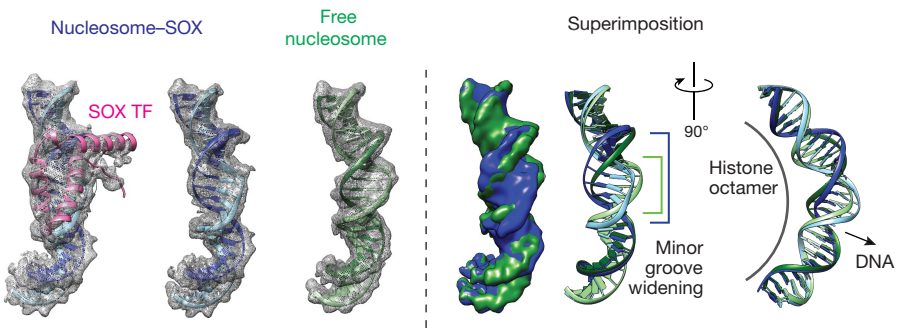

Fig. 2 | Structure of the nucleosome–SOX11 complex, and local DNA distortion. SOX11 is shown in pink, and DNA bound by SOX is shown in dark and light blue. DNA in the free nucleosome structure is shown in dark and light green. The cryo-EM maps shown here were Gaussian-smoothened. For clarity, SOX density was segmented out on the right (blue models). TF, transcription factor.

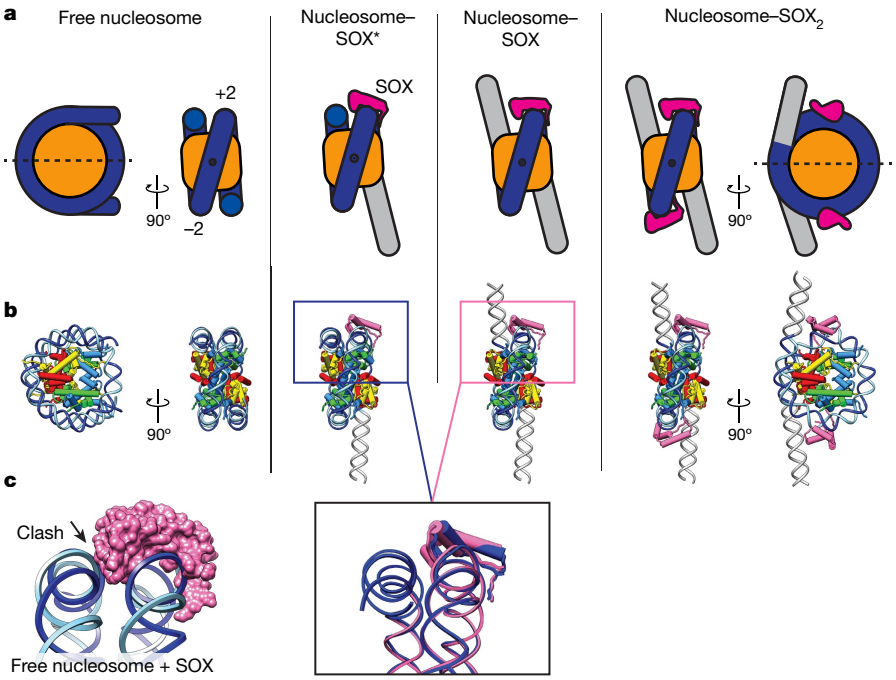

Fig. 3 | Model of nucleosome invasion by SOX factors. a, Nucleosome invasion by SOX factors and terminal DNA detachment. Schematic of the structures reported here. From left to right, free nucleosome, nucleosome–SOX11*, nucleosome–SOX11 and nucleosome–SOX11$_2$ are shown. The histone octamer is shown in orange, SOX in pink and DNA in blue. Detached DNA is shown in grey. The dyad is shown as a dashed line or as a dot. **b**, Four structures, coloured as in Fig. 1. Detached DNA was modelled as ideal B-DNA (grey). The black box shows a comparison of the nucleosome–SOX* (dark blue) and nucleosome–SOX (pink) structures. **c**, DNA superposition in the free nucleosome and the SOX factor (surface view) from the nucleosome–SOX structure illustrates the clash between SOX and the second DNA gyre.

the nucleosome dyad in vivo[24]. However, the possibility that SOX factors may also bind additional nucleosomal positions in other contexts is not excluded.

The nucleosome–SOX11 structure further shows that binding of SOX11 repositions the N-terminal tail of H4 (Fig. 4, Extended Data Fig. 8). In the free nucleosome structure, the H4 tail binds to its canonical site and follows a trajectory towards DNA at SHL +2. However, in the nucleosome–SOX11 structure, the binding site of the H4 tail at SHL +2 is occupied by the SOX11 C-terminal tail (Fig. 4, Extended Data Fig. 8). The H4 tail is displaced, rotated by about 90° and extends towards SHL +1. The functionally important residue lysine 16 (K16) moves by around 33 Å. However, at SHL −2 SOX11 is oriented differently and does not displace the H4 tail (Extended Data Fig. 8c).

We speculate that SOX-factor binding may be incompatible with the formation of canonical nucleosome–nucleosome contacts[28] (Extended Data Fig. 8). Formation of nucleosome arrays depends on the H4 tail and is impaired by K16 acetylation or tail truncation[29–31]. Nucleosome stacking is mediated by H4 tail residues K16–R19 that interact with the acidic patch of the H2A–H2B histone dimer of the neighbouring nucleosome[21,32]. Modelling the SOX DBD onto a nucleosome array[32] suggests that the pioneer factor could be accommodated. SOX binding at SHL +2 and SHL −2 might be preferred over binding at the nucleosome dyad, which would be occluded by the H1 linker histone. However, for efficient chromatin opening, SOX factors cooperate with other transcription factors such as OCT4, KLF4, PAX6, Nanog, BRN2, and PRX1[16], and with ATP-consuming chromatin remodellers[33].

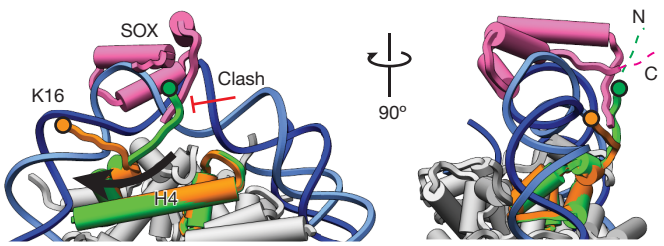

Fig. 4 | SOX11 repositions the H4 tail. Top and side views of SHL +2 with SOX transcription factor (pink). Histones are grey, except for H4. H4 from the free nucleosome is shown in green where the H4 N-terminal (N) tail would clash with the C-terminal (C) SOX tail. In the nucleosome–SOX structure, the H4 tail is repositioned (orange). Residue K16 is marked with a coloured circle.

Online content

Any methods, additional references, Nature Research reporting summaries, source data, extended data, supplementary information, acknowledgements, peer review information; details of author contributions and competing interests; and statements of data and code availability are available at https://doi.org/10.1038/s41586-020-2195-y.

1. Iwafuchi-Doi, M. & Zaret, K. S. Cell fate control by pioneer transcription factors. *Development* **143**, 1833–1837 (2016).
2. Takahashi, K. & Yamanaka, S. Induction of pluripotent stem cells from mouse embryonic and adult fibroblast cultures by defined factors. *Cell* **126**, 663–676 (2006).
3. Adachi, K., Suemori, H., Yasuda, S. Y., Nakatsuji, N. & Kawase, E. Role of SOX2 in maintaining pluripotency of human embryonic stem cells. *Genes Cells* **15**, 455–470 (2010).
4. Lambert, S. A. et al. The human transcription factors. *Cell* **172**, 650–665 (2018).
5. Fuda, N. J., Ardehali, M. B. & Lis, J. T. Defining mechanisms that regulate RNA polymerase II transcription *in vivo*. *Nature* **461**, 186–192 (2009).
6. Wang, J. et al. Sequence features and chromatin structure around the genomic regions bound by 119 human transcription factors. *Genome Res.* **22**, 1798–1812 (2012).
7. Zhu, F. et al. The interaction landscape between transcription factors and the nucleosome. *Nature* **562**, 76–81 (2018).
8. Cirillo, L. A. et al. Opening of compacted chromatin by early developmental transcription factors HNF3 (FoxA) and GATA-4. *Mol. Cell* **9**, 279–289 (2002).
9. Boller, S., Li, R. & Grosschedl, R. Defining, B cell chromatin: lessons from EBF1. *Trends Genet.* **34**, 257–269 (2018).
10. Chen, J. et al. Single-molecule dynamics of enhanceosome assembly in embryonic stem cells. *Cell* **156**, 1274–1285 (2014).

11. Velychko, S. et al. Excluding Oct4 from Yamanaka cocktail unleashes the developmental potential of iPSCs. *Cell Stem Cell* **25**, 737–753.e4 (2019).
12. Soufi, A. et al. Pioneer transcription factors target partial DNA motifs on nucleosomes to initiate reprogramming. *Cell* **161**, 555–568 (2015).
13. Meers, M. P., Janssens, D. H. & Henikoff, S. Pioneer factor–nucleosome binding events during differentiation are motif encoded. *Mol. Cell* **75**, 562–575.e5 (2019).
14. Malik, V. et al. Pluripotency reprogramming by competent and incompetent POU factors uncovers temporal dependency for Oct4 and Sox2. *Nat. Commun.* **10**, 3477 (2019).
15. Biddle, J. W., Nguyen, M. & Gunawardena, J. Negative reciprocity, not ordered assembly, underlies the interaction of Sox2 and Oct4 on DNA. *eLife* **8**, e41017 (2019).
16. Kamachi, Y. & Kondoh, H. Sox proteins: regulators of cell fate specification and differentiation. *Development* **140**, 4129–4144 (2013).
17. Badis, G. et al. Diversity and complexity in DNA recognition by transcription factors. *Science* **324**, 1720–1723 (2009).
18. Jauch, R., Ng, C. K., Narasimhan, K. & Kolatkar, P. R. The crystal structure of the Sox4 HMG domain–DNA complex suggests a mechanism for positional interdependence in DNA recognition. *Biochem. J.* **443**, 39–47 (2012).
19. Bergsland, M. et al. Sequentially acting Sox transcription factors in neural lineage development. *Genes Dev.* **25**, 2453–2464 (2011).
20. Wiebe, M. S., Nowling, T. K. & Rizzino, A. Identification of novel domains within Sox-2 and Sox-11 involved in autoinhibition of DNA binding and partnership specificity. *J. Biol. Chem.* **278**, 17901–17911 (2003).
21. Luger, K., Mäder, A. W., Richmond, R. K., Sargent, D. F. & Richmond, T. J. Crystal structure of the nucleosome core particle at 2.8 A resolution. *Nature* **389**, 251–260 (1997).
22. Williams, D. C., Jr, Cai, M. & Clore, G. M. Molecular basis for synergistic transcriptional activation by Oct1 and Sox2 revealed from the solution structure of the 42-kDa Oct1.Sox2. Hoxb1–DNA ternary transcription factor complex. *J. Biol. Chem.* **279**, 1449–1457 (2004).
23. Voong, L. N. et al. Insights into nucleosome organization in mouse embryonic stem cells through chemical mapping. *Cell* **167**, 1555–1570.e15 (2016).
24. Li, S., Zheng, E. B., Zhao, L. & Liu, S. Nonreciprocal and conditional cooperativity directs the pioneer activity of pluripotency transcription factors. *Cell Rep.* **28**, 2689–2703 (2019).
25. Hall, M. A. et al. High-resolution dynamic mapping of histone–DNA interactions in a nucleosome. *Nat. Struct. Mol. Biol.* **16**, 124–129 (2009).
26. Bilokapic, S., Strauss, M. & Halic, M. Histone octamer rearranges to adapt to DNA unwrapping. *Nat. Struct. Mol. Biol.* **25**, 101–108 (2018).
27. Donovan, B. T., Chen, H., Jipa, C., Bai, L. & Poirier, M. G. Dissociation rate compensation mechanism for budding yeast pioneer transcription factors. *eLife* **8**, e43008 (2019).
28. Pepenella, S., Murphy, K. J. & Hayes, J. J. Intra- and inter-nucleosome interactions of the core histone tail domains in higher-order chromatin structure. *Chromosoma* **123**, 3–13 (2014).
29. Gordon, F., Luger, K. & Hansen, J. C. The core histone N-terminal tail domains function independently and additively during salt-dependent oligomerization of nucleosomal arrays. *J. Biol. Chem.* **280**, 33701–33706 (2005).
30. Shogren-Knaak, M. et al. Histone H4-K16 acetylation controls chromatin structure and protein interactions. *Science* **311**, 844–847 (2006).
31. Dorigo, B., Schalch, T., Bystricky, K. & Richmond, T. J. Chromatin fiber folding: requirement for the histone H4 N-terminal tail. *J. Mol. Biol.* **327**, 85–96 (2003).
32. Song, F. et al. Cryo-EM study of the chromatin fiber reveals a double helix twisted by tetranucleosomal units. *Science* **344**, 376–380 (2014).
33. Engelen, E. et al. Sox2 cooperates with Chd7 to regulate genes that are mutated in human syndromes. *Nat. Genet.* **43**, 607–611 (2011).

Methods

No statistical methods were used to predetermine sample size. The experiments were not randomized and investigators were not blinded to allocation during experiments and outcome assessment.

Plasmids and strains

Full-length histone sequences from *Homo sapiens* were incorporated into the following plasmids: pET22B-H2B, pET22b-H3.2, pET3a-H4 (kindly provided by the W. Fischle laboratory). The H2A construct was cloned into a LIC1B vector (MacroLabs) and contained an N-terminal 6×His-tag followed by a tobacco etch virus (TEV) protease cleavage site (HHHHHHENLYFQS). The SOX2 DBD construct contained residues 36–121 of the full-length SOX2 (UniProt ID P48431). The DBD sequence was codon-optimized and synthesized by IDT as a gBlock. The gBlock was inserted into a LIC1B plasmid following N-terminal 6×His-tag and a TEV protease cleavage site sequences. The SOX11 DBD with short flanking sequences contained residues 33–138 of full-length SOX11 (UniProt ID P35716). It was inserted into a LIC1B plasmid. The construct was identical to the SOX11 construct used in a previous study[7]. Protein constructs are schematically shown in Extended Data Fig. 2.

Protein purification

Histones were purified according to standard protocols[34,35]. Purified histones were flash-frozen and lyophilized. Histones were resuspended in unfolding buffer (6 M guanidine hydrochloride, 20 mM HEPES pH 7.5, 10 mM dithiothreitol (DTT)). H2A, H2B, H3 and H4 were mixed in 1.2:1.2:1:1 ratios, and dialysed against three changes of refolding buffer high (RB high: 20 mM HEPES pH 7.5, 1 mM EDTA, 2 M NaCl, 2 mM DTT). After dialysis, the sample was concentrated and loaded onto a size-exclusion chromatography column (Superdex 200 10/300 GL, GE Healthcare). A peak corresponding to the complete octamer was collected and used for nucleosome reconstitution. The SOX2 DBD was expressed in BL21 (DE3) RIL *Escherichia coli* cells and purified over a sequence of columns: affinity His-Trap HP, cation exchange HiTrap SP-HP and size-exclusion Superdex75 10/300 GL (GE Healthcare). The His-tag was cleaved off after the affinity purification step. The SOX11 DBD was expressed and purified exactly as the SOX2 DBD. Purified proteins in the final buffer (20 mM HEPES pH 7.5, 1 mM EDTA, 150 mM NaCl, 1 mM DTT) were flash-frozen and stored at −80°.

DNA preparation

DNA-1 template sequence was: ATCTACACGACGCTCTTCCGATCTAATTT ATGTTTGTTAGCGTTATACTATTCTAATTCTTTGTTTCGGTGGTATTGTTT ATTTTGTTCCTTTGTGCGTTCAGCTTAATGCCTAACGACACTCGGAGAT CGGAAGAGCACACGTGAT. This sequence was directly (no changes) adopted from the NCAP-SELEX experiment with nucleosomes and SOX transcription factor described previously[7].

DNA-1a sequence with all but one of the TTGT motifs replaced by a random sequence was: ATCTACACGACGCTCTTCCGATCTAATTTATTCAG ACTAGCGTTATACTATTCTAATTTCAGACTTCGGTGGTCAGACTTATCAG ACTCCTTTGTGCGTTCAGCTTAATGCCTAACGACACTCGGAGATCGG AAGAGCACACGTGAT.

Widom 601 DNA template used as a control was: ATCGAGAATCCC GGTGCCGAGGCCGCTCAATTGGTCGTAGACAGCTCTAGCACCGCTTA AACGCACGTACGCGCTGTCCCCCGCGTTTTAACCGCCAAGGGGATTA CTCCCTAGTCTCCAGGCACGTGTCAGATATATACATCCGAT. Three bases at each end were changed to accommodate an EcoRV restriction site.

The DNA* template used for the nucleosome–SOX* structure determination was 151 bp long and almost identical to the DNA-1: A TC**CC**TACACGACGCTCTTCCGATCTAATTTATGTTTGTTAGCGTTATAC TATTCTAATTCTTTGTTTCGGTGGTATTGTTTATTTTGTTCCTTTGTGC GTTCAGCTTAATGCCTAACGACACTCGGAGATCGGAAGAGCACACGT**C T**GAT. Two additional nucleotides on each side in the DNA* template are highlighted in bold. The rational for using a slightly longer 151-bp DNA construct was the following. The H2A C-terminal tail regulates nucleosome conformation by binding to linker DNA at different locations and stabilizes the nucleosome[36]. When a longer DNA construct is used, the H2A C-terminal tail stabilizes the DNA ends better (in comparison with the shorter constructs), thus shifting the equilibrium towards a 'closed' nucleosome conformation even in presence of SOX transcription factor.

The 'Widom+1' DNA template had the following sequence: ATCG AGAATCCCGGTGCCGAGGCCGCTCAATTGGTCGTAGACAGCTCTAGC ACCGCTTAAACGCACGTACGCGCTGTCCCCCGCGTTTTTCCTTTGTG CGTTATTACTCCCTAGTCTCCAGGCACGTGTCAGATATATACATCCGAT. The DNA-1b template with all of the TTGT motifs mutated had the following sequence: ATCTACACGACGCTCTTCCGATCTAATTT ATTCAGACTAGCGTTATACTATTCTAATTTCAGACTTCGGTGGTCAGAC TTATCAGACTCTCAGACGCGTTCAGCTTAATGCCTAACGACACTCGGAG ATCGGAAGAGCACACGTGAT.

A plasmid pMK containing four consecutive copies of a DNA template of interest separated by EcoRV restriction sites was ordered from GeneArt (Thermo Fisher). The plasmid was produced in large quantities in *E. coli* XL1 blue cells, and purified with a NucleoBond PC 10000 kit (Macherey Nagel). The plasmid was digested with EcoRV enzyme (NEB) overnight, and produced four copies of the insert per plasmid. The plasmid was then precipitated with PEG-6000[37]. The insert was further purified by size-exclusion chromatography with a Superose 6 Increase column (GE Healthcare). Peak fractions were pooled and concentrated by ethanol precipitation. Alternatively, DNA templates (DNA-1b, Widom+1 and Cy3-labelled DNA-1) were amplified from a plasmid with one insert copy via PCR. PCR product was purified via anion exchange on Resource Q 6 ml column (GE Healthcare).

Sample preparation and experiments for Förster resonance energy transfer

H2A(K119C) was prepared as described above and labelled according to ref. [38] with Cy5–maleimide (GE GEPA25031). Fluorescent DNA-1 template was produced by PCR with a Cy3 5′ labelled primer (IDT). Nucleosomes containing both labelled or just the donor Cy3 as control were reconstituted. Cy3 label was located at the SHL +7 end of the nucleosome. In the buffer containing 10 mM HEPES pH 7.5, 1 mM $MgCl_2$, 0.01 mM $ZnCl_2$, 1 mM DTT, 10 mM NaCl, 0.5 mg/ml BSA, nucleosomes (60 nM concentration) and SOX were mixed on ice and the spectra were recorded. Excitation wavelength of 510 nm was used. Förster resonance energy transfer (FRET) efficiency was calculated using a standard formula $E = 1 - I_{DA}/I_D$. Four independent experiments were performed.

Nucleosome reconstitution

Nucleosomes were reconstituted from the histone octamer and DNA template with a salt gradient as previously described[35]. In brief, octamer and DNA were mixed in 1.2:1 ratio in RB high, transferred into Slide-A-Lyzer MINI Dialysis Units 7,000 MWCO (Thermo Fisher), and dialysed gradually over a course of 24 h from RB high into RB low (20 mM HEPES pH 7.5, 1 mM EDTA, 20 mM NaCl, 2 mM DTT). Freshly reconstituted nucleosomes were concentrated in Amicon Ultra-0.5 centrifugal filters MWCO 10,000 (Sigma Aldrich).

Cryo-EM grid preparation and data collection

Nucleosomes at 1.6 μM concentration were mixed with 20× molar excess of SOX transcription factor at 4 °C in the final buffer containing 20 mM HEPES pH 7.5, 1 mM EDTA, 30 mM NaCl, 2 mM DTT, and used for cryo-grid preparation. First, R 2/1 Cu 300 mesh grids (Quantifoil) were glow-discharged with PELCO easiGlow (Ted Pella) device for 120 s. Next, 3.5 μl of sample was applied to the grid in the Vitrobot Mark IV (FEI) chamber at 100% humidity and 16 °C. The excess of liquid was blotted away for 10 s, and the grid was vitrified by plunging into liquid ethane. Data collection was performed on a G2 Titan Krios microscope (FEI) equipped with a K2 Summit direct electron detector (Gatan). Data were collected with EPU software (Thermo Fisher), with defocus ranging

from 0.9 to 3.4 µm at a nominal magnification of 130,000× and a pixel size of 1.05 Å/pixel. Data were collected with an energy filter slit set to 30 eV. The total electron dose of 45 e^-/A^2 was distributed over 40 movie frames. For all imaged samples at least 50% of the data were collected at 25° stage tilt to partially compensate for preferred orientation of particles on the grid, and to improve angular distribution. The quality of the reconstructions was improved compared to the zero-tilt data. Data collection was monitored on-the-fly with Warp[39] and cryoSPARC 2D classification[40].

Data processing and analysis

Processing details are summarized in Extended Data Table 1. For every dataset, particles were picked with gAutomatch, CTF determination was performed with Gctf[41]. The initial reference from the free-nucleosome set was obtained ab initio in cryoSPARC, low-pass-filtered to 40 Å and used as a starting point for the 3D classification of all datasets. For every dataset, to speed up the computation, binned particles with the pixel size of 4.2 Å were extracted and subjected to several rounds of 2D classification and 3D classification in Relion[42]. Classes showing high-resolution features were selected for further processing. Next, selected particles were re-extracted with a pixel size of 2.1 Å, and were 3D-classified and cleaned again. Finally, particles were re-extracted at the final pixel size of 1.05 Å and box size of 400 pixels, and subjected to 3D refinement. For all datasets, processing was performed without symmetry application (C_1). Final Fourier shell correlation (FSC) curves supplied with directional FSC curves and anisotropy estimates were calculated using 3DFSC server[43] (Extended Data Fig. 4). In addition, for each map local resolution was calculated in Relion (Extended Data Fig. 4).

For the free nucleosome dataset, after CTF refinement and 3D refinement, final maps were sharpened using *B*-factor of −75. The final dataset contained 368,270 particles. When classified, this dataset showed typical levels of partial DNA unwrapping (about 10 bp) at the nucleosome entry or exit sites in around 15% of the data (similarly to ref. [26]); however, the overwhelming majority of particles contributed to a fully wrapped nucleosome reconstruction.

In case of the nucleosome–SOX2 dataset, classes that showed additional densities were selected after 3D classification (with global soft mask applied). Next, a selected subset was subjected to a round of focused classification with a small soft spherical mask centred at the additional density near SHL +2 of the nucleosome. A class showing strong additional density was selected and further refined. The final dataset was CTF-refined to compensate for local defocus variations. As a final step, the dataset was subjected to non-uniform refinement in cryoSPARC, which led to an improved local resolution distribution in the 3D reconstruction. The final map was sharpened using a *B*-factor of −100. The final dataset contained 32,301 particles. For an overview of the processing pipelines for both nucleosome–SOX11 datasets, see Extended Data Figs. 9, 10. The starting number of particles (several million) was similar for nucleosome–SOX2 and for nucleosome–SOX11 datasets; however, nucleosome–SOX2 yielded a smaller number of 'good' particles that resulted in a final reconstruction.

The nucleosome–SOX11 dataset was processed in a similar way. The final dataset after initial steps of coarse cleaning was classified into four classes, out of which two were of high quality. One of the classes (202,142 particles) showed a clear additional density at SHL +2 and detached terminal DNA. The corresponding final map was sharpened using a *B*-factor of −100. Another class with two additional densities (nucleosome–$SOX11_2$) contained 114,104 particles. It was refined and sharpened using a *B*-factor of −120. In this nucleosome–$SOX11_2$ structure, the SOX factor molecules are located at SHL +2 and SHL −2, but are not related by the two-fold pseudo-symmetry of the nucleosome. This confirms that the density for the second SOX factor is not an artefact of particle misalignment during data processing. Lower occupancy of SOX11 at SHL −2 may be due to the presence of a weaker binding motif TTCT in that position. The local curvature induced by SOX binding at SHL −2 is not as pronounced as at SHL +2, possibly also owing to a weaker binding motif.

The nucleosome–SOX11* dataset resulted in two distinct classes. The first class (130,870 particles) resulted in a map virtually identical to the nucleosome–SOX structure, but with slightly lower resolution (about 4.0 Å). The remaining 63,821 particles resulted in the nucleosome–SOX* map. The final nucleosome–SOX* map was sharpened using *B*-factor of −100.

Model fitting and refinement

To model the free nucleosome structure, we started from a canonical nucleosome structure obtained by cryo-EM (PDB code 6FQ5)[44] and altered the DNA sequence to correspond to the DNA-1 template using Chimera[45]. Several amino acid residues in the *Xenopus laevis* histones were substituted with ones corresponding to the *H. sapiens* histones in Coot[46]. Next, the model was fitted into the corresponding sharpened cryo-EM map of the free nucleosome and refined in real space using Phenix[47].

The refined model of the free nucleosome was used to generate models for the nucleosome–SOX complex structures. In case of the nucleosome–SOX2 complex, both the nucleosome model and the SOX2 structure (PDB code 1O4X) were placed into the cryo-EM map, nucleosome DNA regions outside of the map were removed and the model was refined in real space using Phenix. For the nucleosome–SOX11 models, the nucleosome and the X-ray structure of SOX11 (determined in this study) were placed into the density and refined in real space using Phenix. In both cases, extra reference model restraints ($\sigma = 1$) were imposed to keep the model close to the available higher-resolution X-ray structure. In addition, base-pair and base-stacking restraints were used during refinements, excluding the region near the SOX transcription-factor binding site because strong local DNA distortion was evident in this region of the map. An equivalent procedure was used for modelling the other structures described here.

Electrophoretic mobility shift assay

Nucleosomes at a final concentration of 1.1 nM were mixed with purified proteins (SOX2 or SOX11 DBD). The final buffer contained 10 mM HEPES pH 7.5, 1 mM $MgCl_2$, 0.01 mM $ZnCl_2$, 1 mM DTT, 10 mM NaCl, 0.5 mg/ml BSA, 5% glycerol as in ref. [12] (Extended Data Fig. 3). Samples were incubated at 10 min at room temperature, mixed with Novex Hi-Density TBE sample buffer (Thermo Fisher), and loaded onto a 6% TBE PAGE. Electrophoresis was performed at 4 °C at 100 V in 0.5× TBE buffer for 1.5–2 h. Gels were stained with SYBR Gold dye (Thermo Fisher), washed, and imaged with Typhoon 9500 FLA Imager (GE Healthcare Life Sciences).

Electrophoretic mobility shift assays (EMSAs) (Extended Data Fig. 6) were performed identically to the procedure described above, but with higher final glycerol concentration to better observe the effects of point mutations of SOX11 on the nucleosome-binding properties of SOX11 in a wider range of apparent affinities. A control EMSA in the 12% glycerol buffer is shown in Extended Data Fig. 6a, b.

Digestion assay

Two hundred and fifty nanograms of nucleosome or DNA was mixed on ice with increasing amounts of SOX11 in digestion buffer (20 mM HEPES pH 7.5, 30 mM NaCl, 10 mM magnesium acetate, 0.1 mg/ml BSA). Then, 0.125 units of restriction enzyme BfuCI (NEB) was added to each reaction. Samples were incubated at 37 °C for 30 min, and the enzyme was inactivated by incubating at 65 °C for 20 min. Samples were then incubated with proteinase K and urea, and then were loaded onto a 4–20% TBE-gel. Electrophoresis was performed at 180 V in 1× TBE buffer for 40 min. Gels were stained with SYBR Gold dye (Thermo Fisher), washed, and imaged with a Typhoon 9500 FLA Imager (GE Healthcare Life Sciences). Two independent experiments were performed both for the DNA and nucleosome digestion assays. Band intensities for the digestion product were measured in ImageJ according to standard routine[48].

Crystallization and X-ray structure determination

DNA oligonucleotides (TATTGTTTATTTTGTT and AACAAAATAA ACAATA) were synthesized and PAGE-purified by IDT. Complimentary oligonucleotides were annealed by heating to 95 °C and stepwise cooling to 4 °C (1° per 90 s) at a concentration of 1.5 mM. Concentrated purified SOX11 DBD and 16-mer DNA were mixed in 1:1.2 ratio and incubated on ice for 30 min. Crystallization was achieved by the hanging drop vapour diffusion method at 20 °C by mixing 1 µl of sample solution with 1 µl of reservoir solution containing 100 mM NaOAc pH 4.5, 200 mM CaOAc, 17% PEG400. Crystals were cryo-protected by 35% PEG400 (v/v) in the final storage solution and flash-frozen in liquid nitrogen.

X-ray diffraction data were collected at beamline X10SA at the Swiss Light Source using a Pilatus 6M detector. Data were indexed and integrated using XDS and scaled using XSCALE[49]. The structure was solved by molecular replacement with PHASER[50], using the structure of the free SOX2 (PDB code 1GT0[51]) as the search model. The crystals belonged to space group $P6_1$ and diffracted to a resolution of 2.5 Å. The asymmetric unit contained two protein–DNA complexes (Extended Data Fig. 2d). Density modification and model building was carried out with phenix.autobuild and manually completed in Coot. The model was iteratively refined with phenix.refine and outliers were fixed in Coot. The final R_{free} factor was 26%. The final model contained SOX11 residues 46–122 and DNA nucleotides 1–14. Diffraction data and refinement statistics are summarized in Extended Data Table 2.

Estimation of the effect of Mg^{2+} on the nucleosome–SOX11 structure

Because nucleosomes are known to be sensitive to Mg^{2+} concentration, we wanted to test whether Mg^{2+} affects the nucleosome–SOX11 structure. Nucleosomes at 1.6 µM concentration were mixed with 20× molar excess of SOX11 transcription factor at 4 °C in the final buffer containing 20 mM HEPES pH 7.5, 30 mM NaCl, 1 mM DTT supplied with additional 1 mM $MgCl_2$, 0.01 mM $ZnCl_2$, 0.5% glycerol. Such sample buffer resembles the buffer used for our EMSAs except for glycerol and BSA, which should be avoided in cryo-EM samples. Next, we used this sample for cryo-grid preparation. We collected a dataset on the Titan Krios equipped with a K3 Gatan detector, nominal pixel size 1.07 Å. Processing was done similarly to the other datasets described here. The final set contained 93493 particles. After light 3D classification (removing low resolution classes), the cryo-EM map (at 4 Å resolution, with 0.73 sphericity) looked highly similar to our original nucleosome–SOX11 structure. The comparison is shown in the Extended Data Fig. 6g. We concluded that Mg^{2+} ions do not alter nucleosome–SOX structure. Overall, the Mg^{2+} sample looked better than the original one in terms of SOX occupancy and quality: a higher portion of particles from the original set contributed to the final reconstruction. We did not further analyse this dataset.

Reporting summary

Further information on research design is available in the Nature Research Reporting Summary linked to this paper.

Data availability

The cryo-EM density reconstructions and final models have been deposited with the Electron Microscopy Data Bank (EMD-10390, EMD-10391, EMD-10392, EMD-10393 and EMD-10394) and with the Protein Data Bank (PDB) (6T78, 6T79, 6T7A, 6T7B, 6T7C and 6T7D). All data are available in the Article and its Supplementary Information.

34. Luger, K., Rechsteiner, T. J. & Richmond, T. J. Expression and purification of recombinant histones and nucleosome reconstitution. *Methods Mol. Biol.* **119**, 1–16 (1999).
35. Dyer, P. N. et al. Reconstitution of nucleosome core particles from recombinant histones and DNA. *Methods Enzymol.* **375**, 23–44 (2004).
36. Li, Z. & Kono, H. Distinct roles of histone H3 and H2A tails in nucleosome stability. *Sci. Rep.* **6**, 31437 (2016).
37. Lis, J. T. & Schleif, R. Size fractionation of double-stranded DNA by precipitation with polyethylene glycol. *Nucleic Acids Res.* **2**, 383–390 (1975).
38. Shimko, J. C., North, J. A., Bruns, A. N., Poirier, M. G. & Ottesen, J. J. Preparation of fully synthetic histone H3 reveals that acetyl-lysine 56 facilitates protein binding within nucleosomes. *J. Mol. Biol.* **408**, 187–204 (2011).
39. Tegunov, D. & Cramer, P. Real-time cryo-electron microscopy data preprocessing with Warp. *Nat. Methods* **16**, 1146–1152 (2019).
40. Punjani, A., Rubinstein, J. L., Fleet, D. J. & Brubaker, M. A. cryoSPARC: algorithms for rapid unsupervised cryo-EM structure determination. *Nat. Methods* **14**, 290–296 (2017).
41. Zhang, K. Gctf: real-time CTF determination and correction. *J. Struct. Biol.* **193**, 1–12 (2016).
42. Scheres, S. H. RELION: implementation of a Bayesian approach to cryo-EM structure determination. *J. Struct. Biol.* **180**, 519–530 (2012).
43. Tan, Y. Z. et al. Addressing preferred specimen orientation in single-particle cryo-EM through tilting. *Nat. Methods* **14**, 793–796 (2017).
44. Bilokapic, S., Strauss, M. & Halic, M. Structural rearrangements of the histone octamer translocate DNA. *Nat. Commun.* **9**, 1330 (2018).
45. Pettersen, E. F. et al. UCSF Chimera—a visualization system for exploratory research and analysis. *J. Comput. Chem.* **25**, 1605–1612 (2004).
46. Emsley, P., Lohkamp, B., Scott, W. G. & Cowtan, K. Features and development of Coot. *Acta Crystallogr. D* **66**, 486–501 (2010).
47. Adams, P. D. et al. PHENIX: a comprehensive Python-based system for macromolecular structure solution. *Acta Crystallogr. D* **66**, 213–221 (2010).
48. Rueden, C. T. et al. ImageJ2: ImageJ for the next generation of scientific image data. *BMC Bioinformatics* **18**, 529 (2017).
49. Kabsch, W. Xds. *Acta Crystallogr. D* **66**, 125–132 (2010).
50. McCoy, A. J. Solving structures of protein complexes by molecular replacement with Phaser. *Acta Crystallogr. D* **63**, 32–41 (2007).
51. Reményi, A. et al. Crystal structure of a POU/HMG/DNA ternary complex suggests differential assembly of Oct4 and Sox2 on two enhancers. *Genes Dev.* **17**, 2048–2059 (2003).
52. Sievers, F. et al. Fast, scalable generation of high-quality protein multiple sequence alignments using Clustal Omega. *Mol. Syst. Biol.* **7**, 539 (2011).
53. Klaus, M. et al. Structure and decoy-mediated inhibition of the SOX18/Prox1-DNA interaction. *Nucleic Acids Res.* **44**, 3922–3935 (2016).
54. Palasingam, P., Jauch, R., Ng, C. K. & Kolatkar, P. R. The structure of Sox17 bound to DNA reveals a conserved bending topology but selective protein interaction platforms. *J. Mol. Biol.* **388**, 619–630 (2009).
55. Werner, M. H., Huth, J. R., Gronenborn, A. M. & Clore, G. M. Molecular basis of human 46X,Y sex reversal revealed from the three-dimensional solution structure of the human SRY–DNA complex. *Cell* **81**, 705–714 (1995).

Acknowledgements We thank members of the Cramer laboratory, in particular H. Hillen, D. Tegunov, and G. Kokic for advice; the crystallization facility at our institute, in particular J. Wawrzinek and U. Steuerwald; and W. Fischle for providing histone expression constructs. Part of this work was performed at Beamline X10SA at the SLS at the PSI. S.O.D. was supported by an EMBO long-term fellowship (ALTF-949-2016). P.C. was supported by the Deutsche Forschungsgemeinschaft (EXC 2067/1-390729940), the ERC Advanced Investigator Grant TRANSREGULON (grant agreement no 693023) and the Volkswagen Foundation.

Author contributions S.O.D. designed and carried out all experiments and data analysis. F.Z., supported by J.T., identified the original DNA template used in the study. C.D. assisted with cryo-EM data collection. P.C. designed and supervised research. S.O.D. and P.C. interpreted the data and wrote the manuscript, with input from all authors.

Competing interests The authors declare no competing interests.

Additional information

Supplementary information is available for this paper at https://doi.org/10.1038/s41586-020-2195-y.

Correspondence and requests for materials should be addressed to P.C.

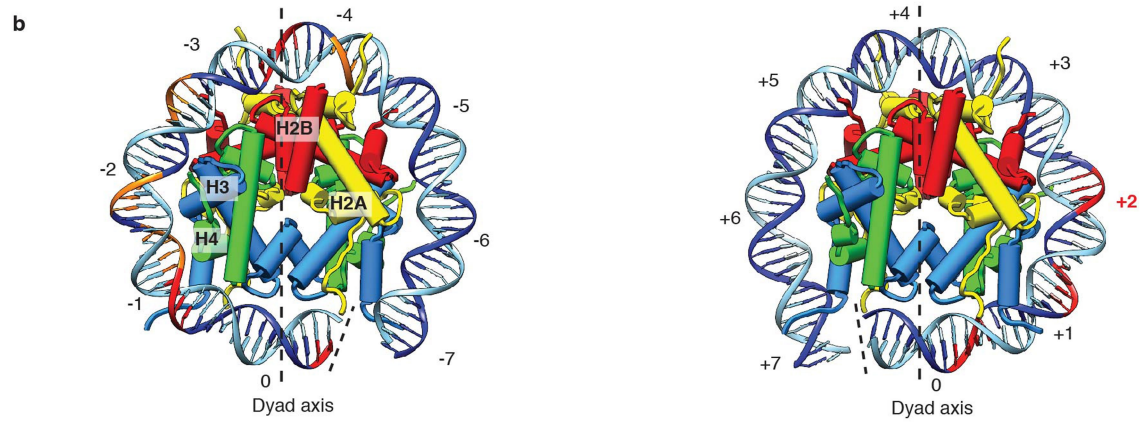

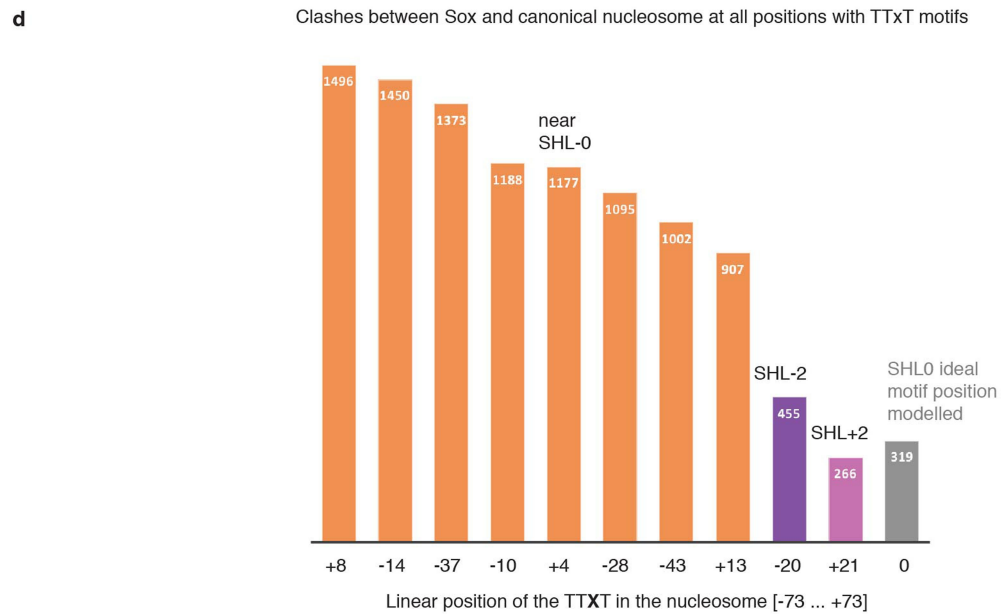

Extended Data Fig. 1 | DNA constructs and motif positions. Related to Fig. 1. **a**, DNA-1 sequence. Two DNA strands are coloured in dark and light blue, canonical core motifs TTGT are coloured in red, TTXT motifs are shown in orange. Only motifs that allow SOX binding to the DNA minor groove are considered. The position of the third nucleotide of each motif in the DNA-1 sequence is indicated. Motifs at SHL+2 and −2 are shown in bold. **b**, Top views of the nucleosome. H2A, H2B, H3 and H4 are shown in yellow, red, blue and green, respectively, DNA is shown in dark and light blue. SHLs are labelled. **c**, DNA-1a template sequence. Only one TTGT motif is present (red). **d**, Structure of SOX2 (PDB code 1O4X) was aligned to each of the motifs present in nucleosome 1 and allowing binding of SOX to the minor groove. The number of clashes was calculated using 'findclash' command in Chimera software. SOX2 binding to motifs at SHL +2 and SHL −2 gives rise to the least amount of clashes with DNA and histones compared to other locations. The ideal position (modelled) of the SOX motif on the dyad would result in a comparably low number of clashes.

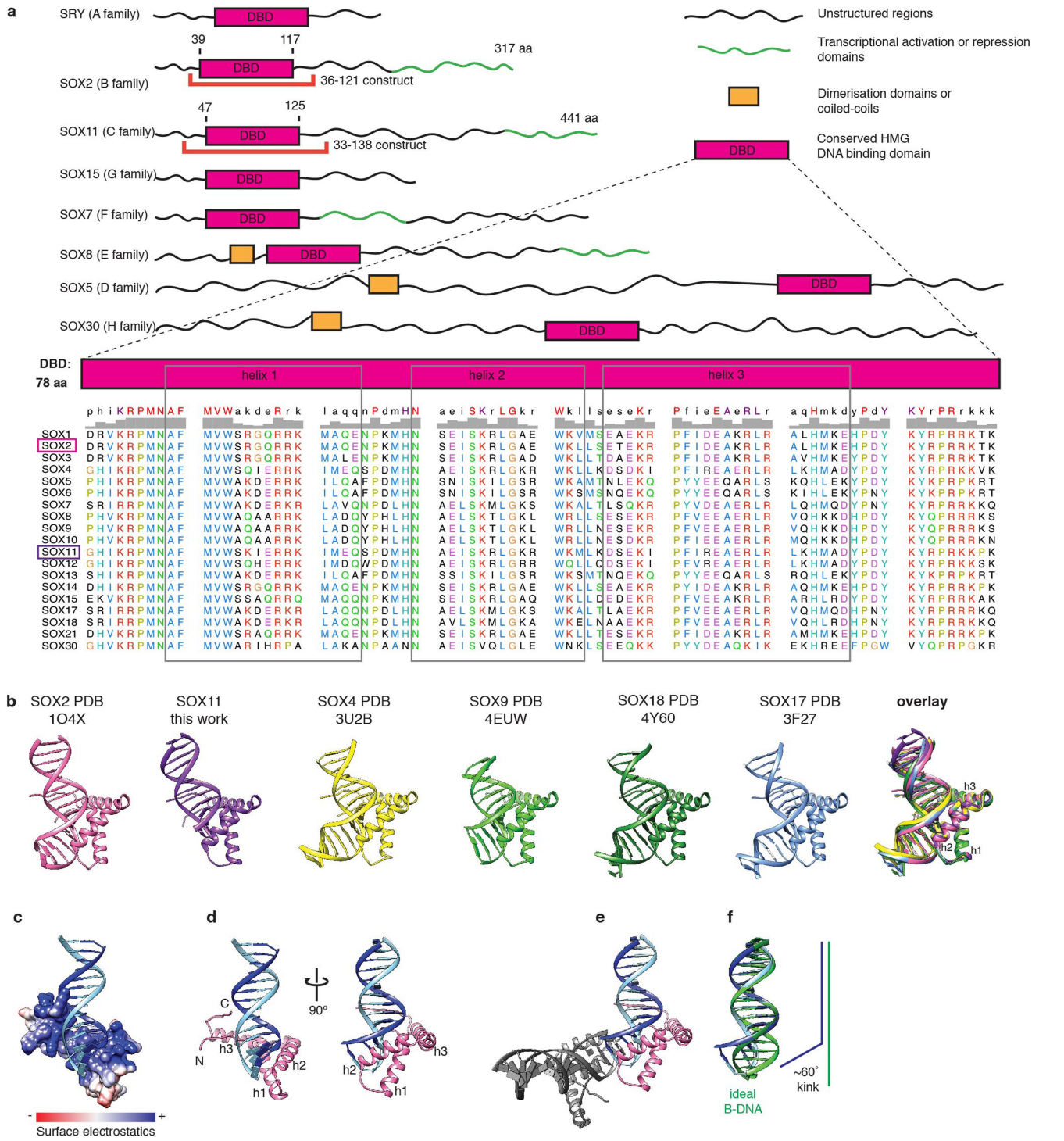

Extended Data Fig. 2 | Conservation of SOX-family DBD sequence and structure, and X-ray structure of the SOX11–DNA complex. Related to Fig. 1. **a**, Domain organization of the human SOX protein family. DBDs are shown as pink rectangles; unstructured functionally diverse regions are shown as wavy lines. Protein constructs used in this study are marked. The alignment of DBD sequences (produced using Clustal Omega) is shown below[52]. **b**, Structural conservation of SOX factors. Crystal and nuclear magnetic resonance structures of SOX transcription factors: SOX2 (ref. [22]), SOX11 (this study), SOX4 (ref. [18]), SOX9, SOX18 (ref. [53]) and SOX17 (ref. [54]); SRY (ref. [55]) has a similar fold. Superimposition of all the structures reveals that they are virtually identical. **c**, DNA is engulfed by the strongly positively charged inner surface of the SOX11 DBD. **d**, Ribbon representation of the SOX11 X-ray structure. **e**, Two copies of SOX11–DNA in the asymmetric unit. The contact between the two is mediated by DNA stacking. **f**, Comparison of the observed DNA conformation with canonical B-DNA (green). SOX11 introduces a kink into DNA that is typical for HMG box proteins.

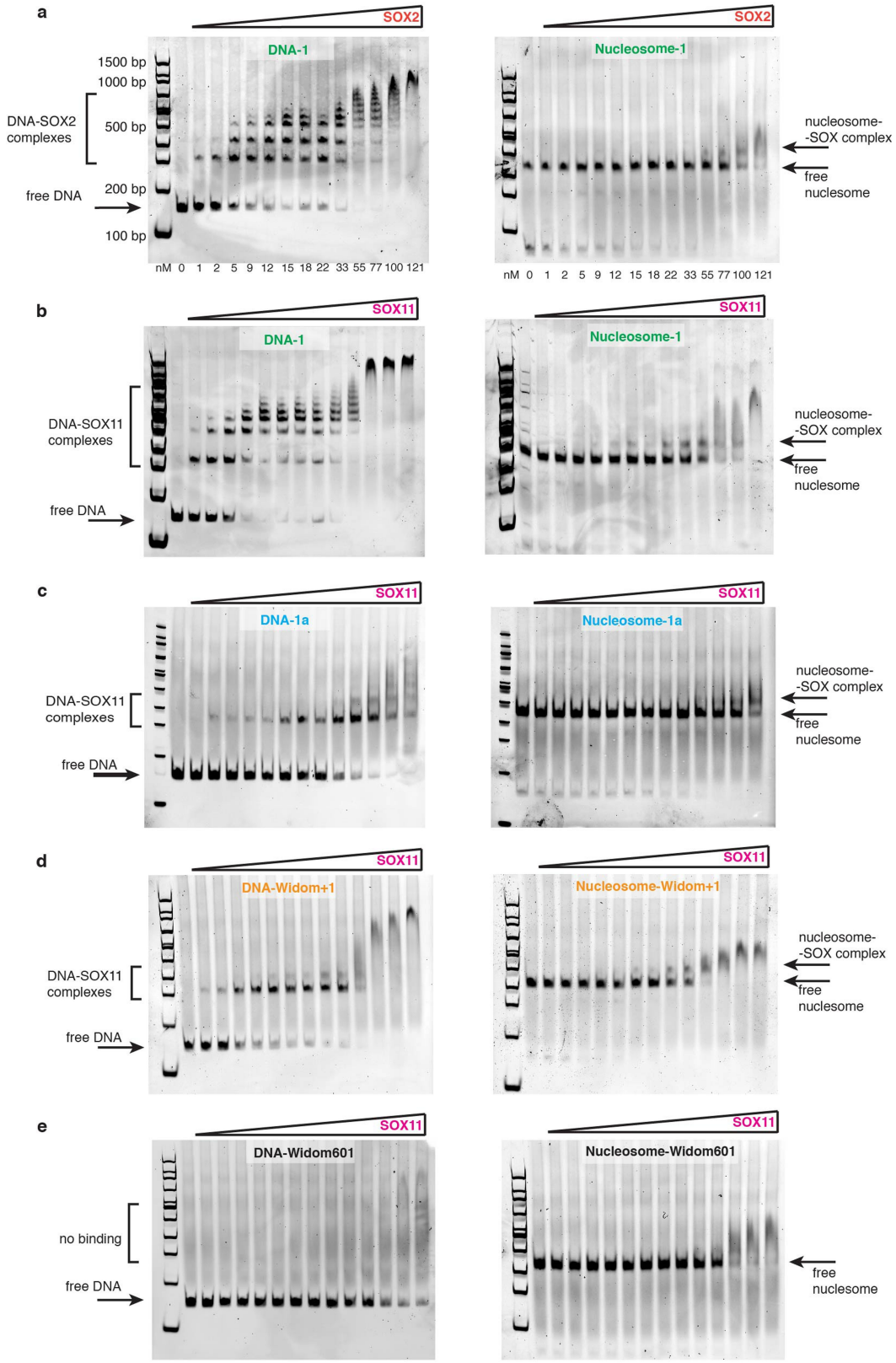

Extended Data Fig. 3 | EMSAs of SOX2 and SOX11 in complex with DNA or nucleosomes. Related to Figs. 1–3. EMSAs reveal formation of SOX-factor complexes with DNA (left) or nucleosomes (right). DNA or nucleosome concentration is 1.1 nM. **a**, EMSA of DNA-1–SOX2 and nucleosome-1–SOX2 complexes. **b**, EMSA of DNA-1–SOX11 and nucleosome-1–SOX11 complexes. **c**, EMSA of DNA-1a–SOX11 and nucleosome-1a–SOX11 complexes. **d**, EMSA of DNA–Widom+1 and nucleosome–Widom+1–SOX11 complexes. **e**, EMSA of DNA Widom 601–SOX11 and nucleosome Widom 601–SOX11 complexes. Relevant bands are labelled. All experiments were repeated at least twice with similar results. For gel source data, see Supplementary Fig. 1.

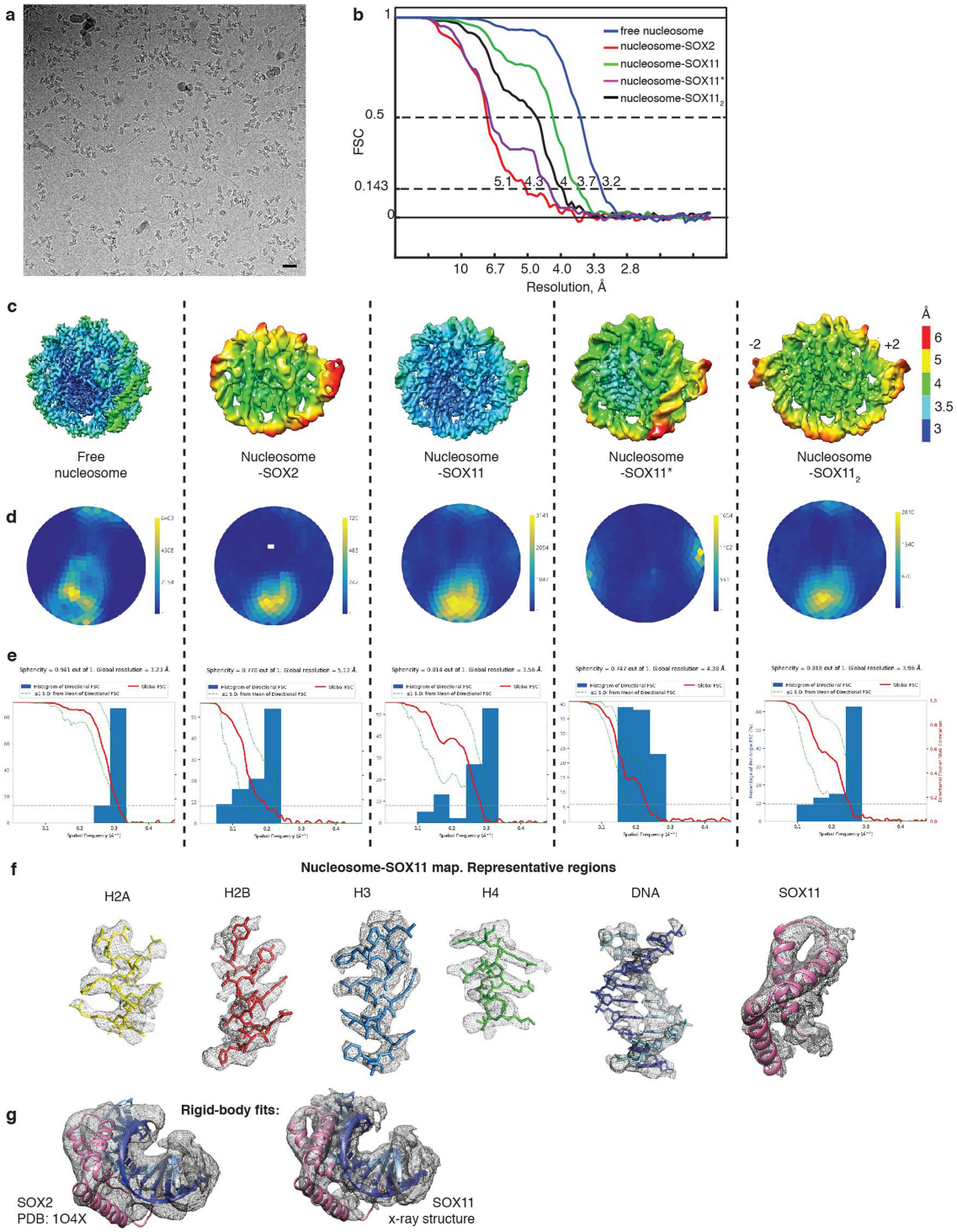

Extended Data Fig. 4 | Global and local resolution of cryo-EM reconstructions. Related to Figs. 1–3. **a**, Example micrograph reveals preferred orientation of nucleosomes. Scale bar, 20 nm. **b**, FSC plots for five reported reconstructions. **c**, Local resolution distribution. In some maps, the resolution varies from 3 Å (dark blue) through 4 Å (green) to 6 Å (red). The lower resolution of some DNA regions indicates flexibility. **d**, Angular distribution plots. Scale shows the number of particles assigned to a particular angle. Blue, a low number of particles; yellow, a high number of particles. **e**, Directional FSC plots for the reconstructions calculated on the 3DFSC server[48]. Sphericity, as the degree of anisotropy present in the reconstructions, is indicated above each plot. Histograms indicate the portion of voxels with a particular resolution. **f**, Visualization of different regions of the nucleosome–SOX11 map. In the nucleosome core, histone side chains are clearly visible; SOX density has a lower resolution, but helical densities are clearly distinguishable. **g**, Rigid-body fit of the SOX2–DNA structure (PDB code 1O4X) into the nucleosome–SOX2 cryo-EM map (left). Rigid-body fit of the SOX11–DNA X-ray structure into the nucleosome–SOX11 cryo-EM map (right). The region containing SOX and a short DNA stretch was isolated from the rest of the map for clarity.

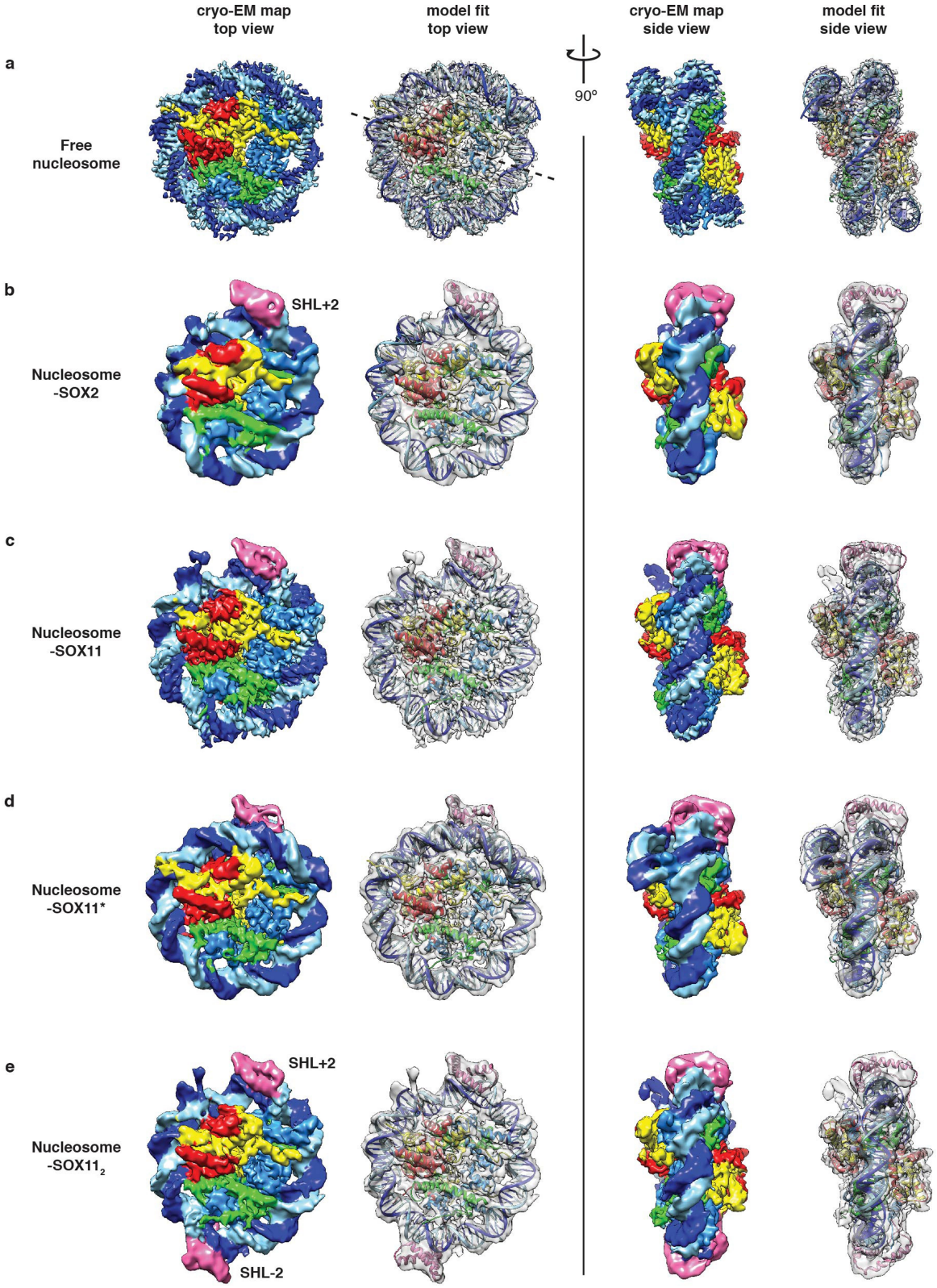

Extended Data Fig. 5 | Gallery of cryo-EM structures. Related to Figs. 1–4. **a**–**e**, Electron microscopy maps and corresponding models of all reported structures. Top views (left) and side views (right) are related by a 90° rotation. The maps are coloured on the basis of the fitted model (as in Fig. 1), or are transparent.

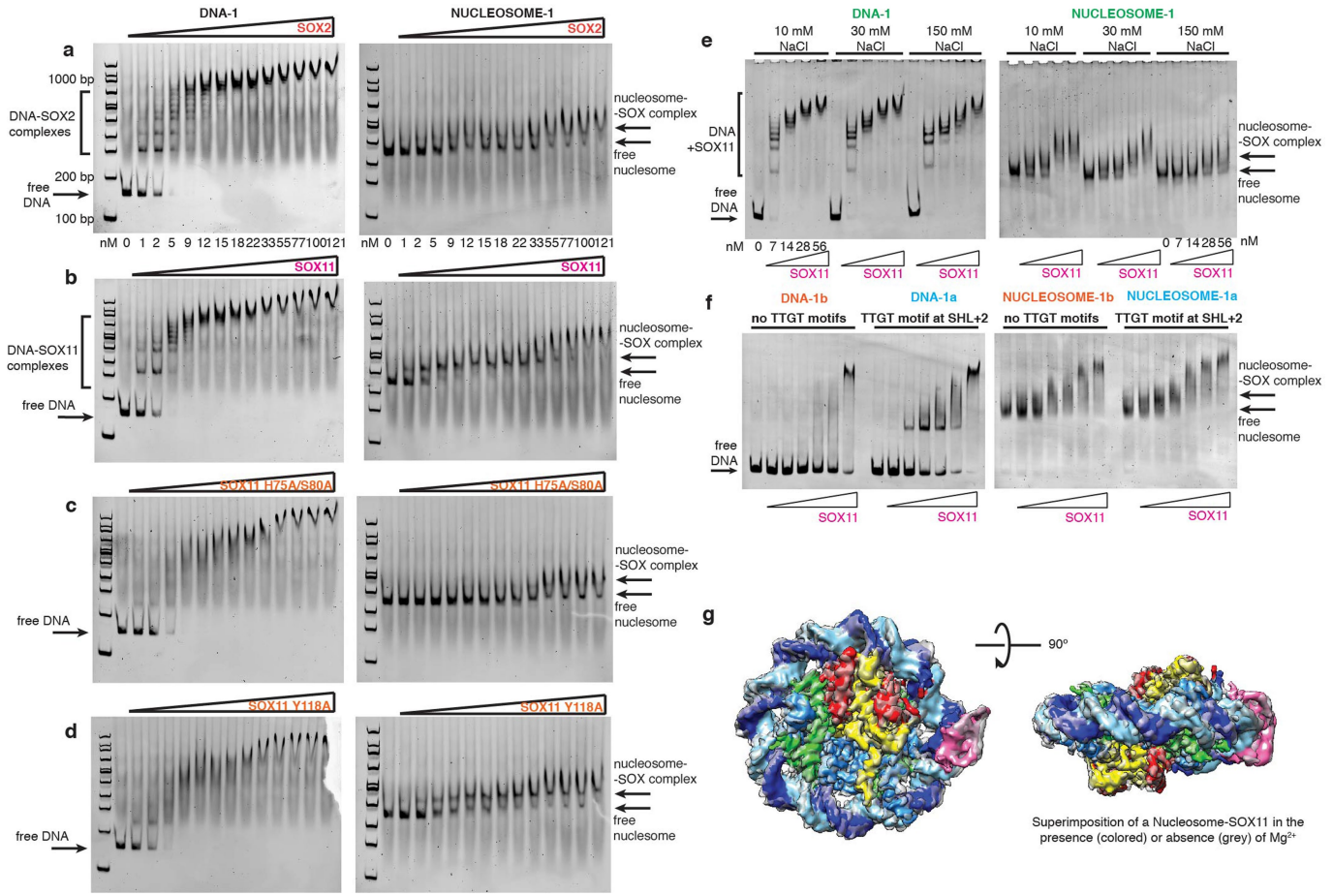

Extended Data Fig. 6 | EMSAs using SOX2, and wild-type or mutant SOX11 in complex with DNA or nucleosomes. Related to Figs. 1–3. EMSAs reveal the formation of SOX-factor complexes with DNA or nucleosomes. All experiments were repeated at least twice with similar results. For gel source data, see Supplementary Fig. 1. **a**, EMSA of DNA-1 or nucleosome-1 with wild-type SOX2. **b**, EMSA of DNA-1 or nucleosome-1 with wild-type SOX11. **c**, EMSA of DNA-1 or nucleosome-1 with SOX11(H75A/S80A). **d**, EMSA of DNA-1 or nucleosome-1 with SOX11(Y118A). Relevant bands are labelled. To observe a wider range of the binding curve for the mutants, a larger amount of glycerol (12% final concentration) was used here (as compared to the EMSAs shown in Extended Data Fig. 3, which used 5% glycerol)—thus, the apparent affinity is higher. DNA or nucleosome concentration is 1.1 nM. **e**, EMSAs reveal formation of SOX–DNA or SOX–nucleosome complexes at different concentrations of salt. There is virtually no difference in binding at 10 or 30 mM NaCl, whereas binding is weaker at 150 mM NaCl. DNA or nucleosome concentration is 1.1 nM. **f**, EMSAs reveal formation of SOX complexes with DNA-1a or nucleosome-1a (only one canonical motif present) as compared to DNA-1b and nucleosome-1b (in which all canonical SOX motifs were mutated). SOX concentrations ranged from 0 to 200 nM, DNA concentration was 1.1 nM. **g**, Superimposition of two nucleosome–SOX11 cryo-EM maps obtained in the presence of 1 mM $MgCl_2$ (grey density) or in the absence of $MgCl_2$ (coloured). Magnesium does not influence the structure of the SOX–nucleosome complex. Cross-correlation between the two unmasked maps is 0.94 (Chimera).

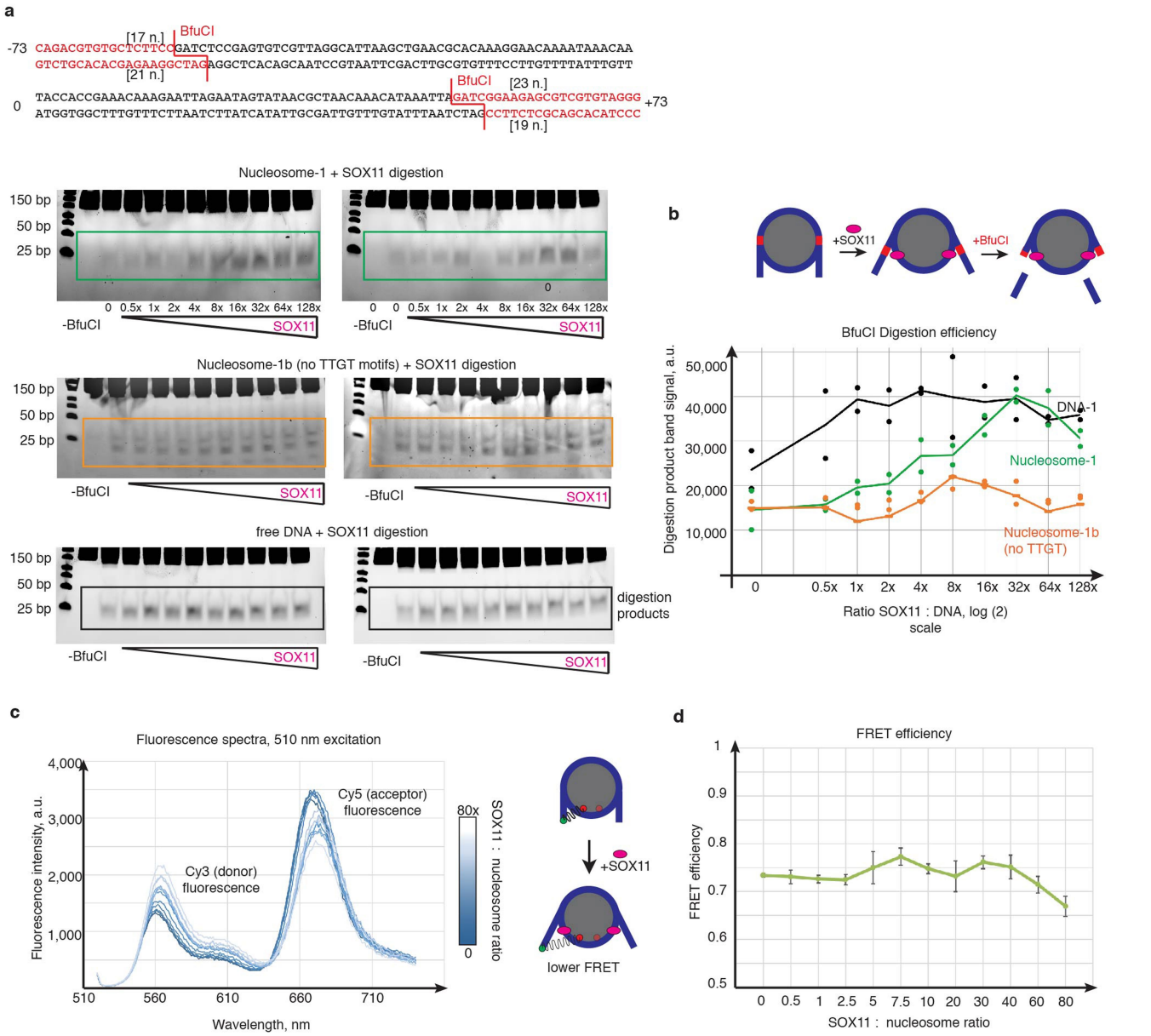

Extended Data Fig. 7 | Nucleosome-DNA end unwrapping. Related to Figs. 1, 3. **a**, DNA-1 sequence with BfuCI digestion sites. BfuCI digestion assays (two independent experiments for each sample, shown here) of the DNA-1, nucleosome-1 or nucleosome-1b (no TTGT motifs) in the presence of increasing amounts of SOX11. The restriction site (about 20 nucleotides away from the entry and exit sites of the nucleosome) becomes more accessible with higher concentrations of SOX11. In a DNA-1 digestion assay, the amount of digestion product increases slightly in the low SOX11 concentration range, and then stays constant over a broad concentration range. For gel source data, see Supplementary Fig. 1. **b**, BfuCI digestion assay plot for free DNA-1 (black), nucleosome-1 (green) and mutated nucleosome-1b (orange) in the presence of increasing amounts of SOX11. Each experiment was performed independently twice ($n = 2$). Mean values (lines) and individual measurements (dots) are shown. Band intensity was calculated using standard routine in ImageJ[52]. **c**, Example fluorescence spectra of Cy3–Cy5-labelled nucleosome in the presence of increasing amounts of SOX11. **d**, FRET efficiency plot. Mean values with s.d. are shown (independent experiments, $n = 4$).

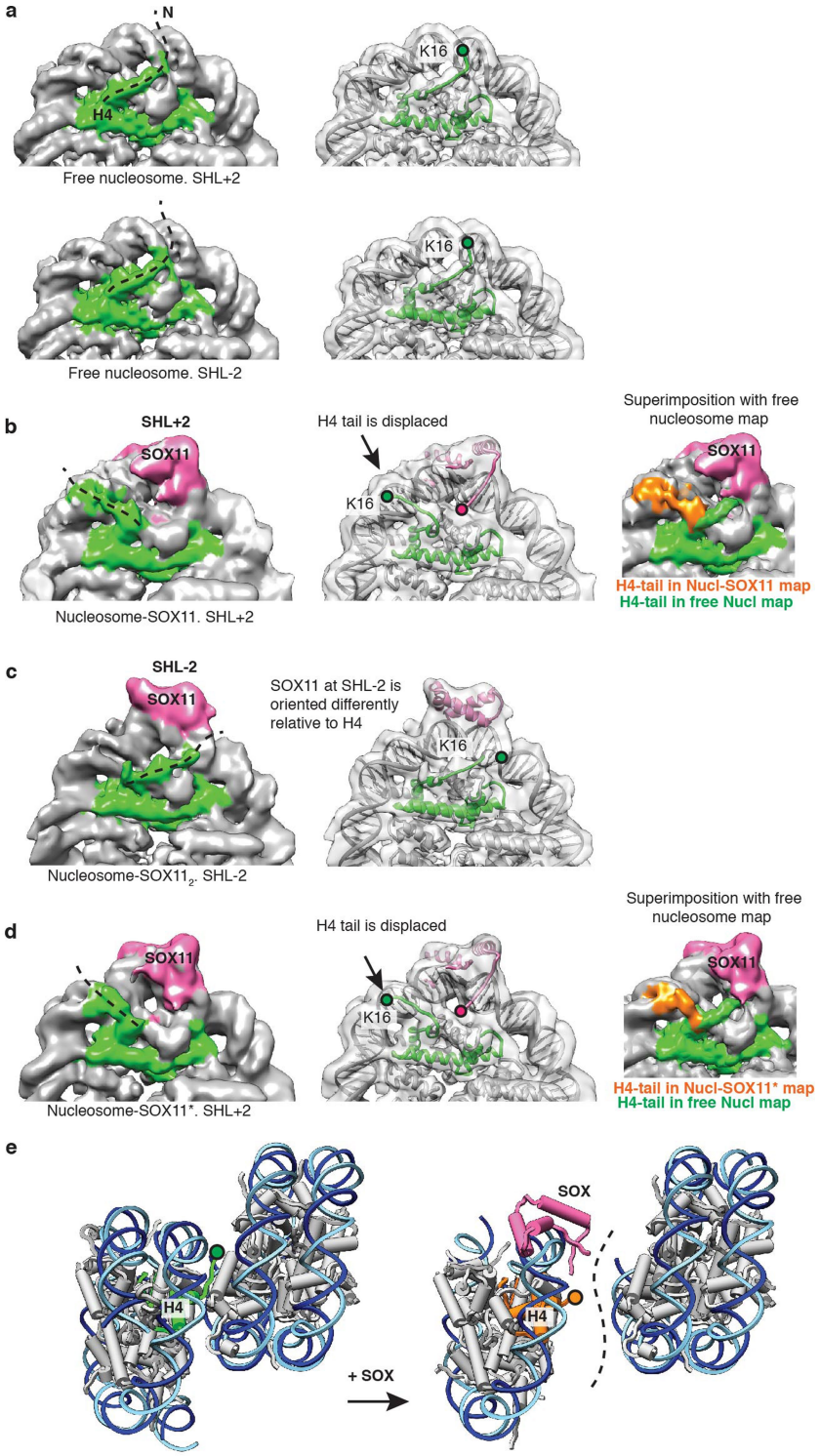

Extended Data Fig. 8 | Repositioning of the H4 N-terminal tail. Related to Fig. 4. Cryo-EM maps are shown with a Gaussian smoothening filter (Chimera[49]) applied for clarity. SOX is coloured in pink, H4 is shown in green and the repositioned H4 tail is shown in orange. **a**, Free nucleosome. Views of SHL +2 and SHL −2 are shown to illustrate the position of the H4 tail (a dashed line). Residue K16 is marked with a circle. **b**, Nucleosome–SOX11 with SOX11 located at SHL +2. On the right, a superimposition with the free nucleosome map is shown to highlight different orientations of the H4 tail. **c**, Nucleosome–SOX11 complex with SOX11 located at SHL −2. In this location, SOX is oriented differently and does not clash with or reposition the H4 tail. **d**, Nucleosome–SOX11*. The H4 N-terminal tail is repositioned compared with that in the free nucleosome. Repositioning of the H4 tail was reported in case of strong distortions in the nucleosome structure[30]. **e**, SOX binding repositions the H4 N-terminal tail and might impair nucleosome stacking. Side view of two stacking nucleosomes (from PDB code 1AOI). H4 interacts with the acidic patch on the neighbouring H2A–H2B histone dimer. H4 tail repositioning is incompatible with nucleosome stacking.

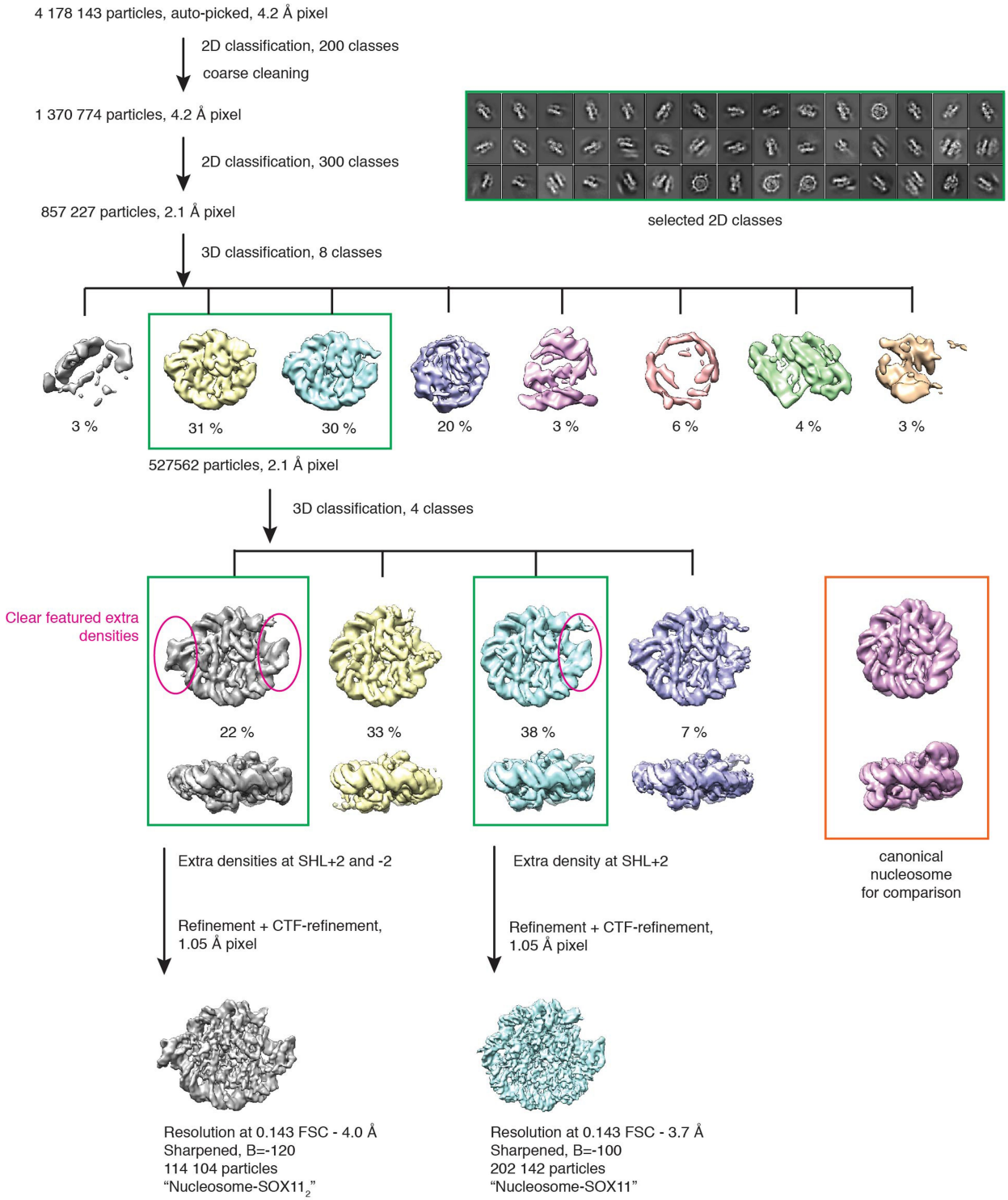

Extended Data Fig. 9 | Flow chart for the determination of the cryo-EM structure of the nucleosome–SOX11$_2$ and nucleosome–SOX11 complexes with 147-bp DNA-1. Related to Figs. 1–3. The processing chart for the 147-bp DNA-1 nucleosome and SOX11 is depicted. The two resulting structures are nucleosome–SOX11$_2$ and nucleosome–SOX11.

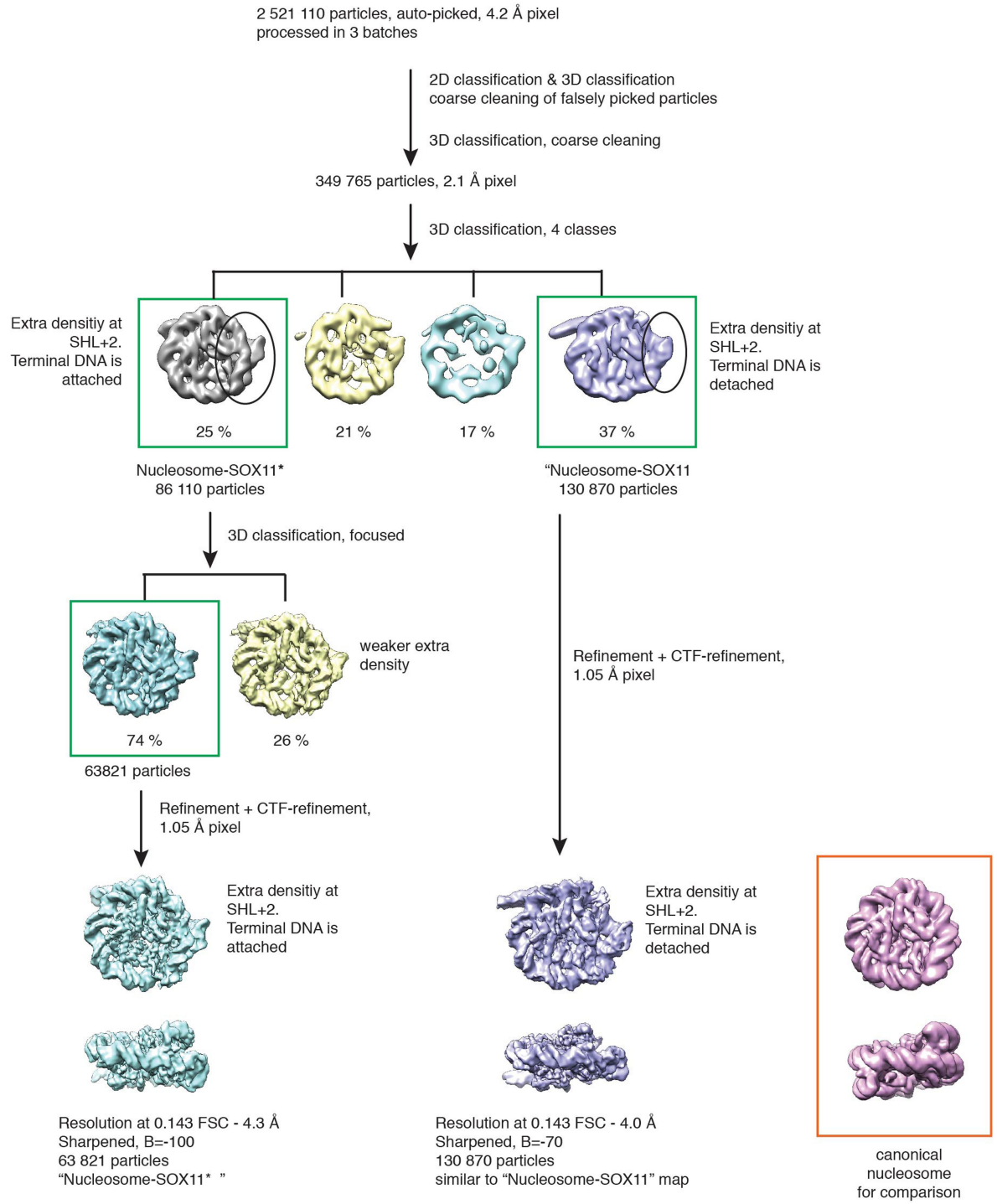

Extended Data Fig. 10 | Flow chart for determination of the cryo-EM structure of the nucleosome–SOX11* complex with 151-bp DNA-1. Related to Figs. 1–3. The processing chart for the 151-bp DNA-1 nucleosome and SOX11 is depicted. The two resulting structures are nucleosome–SOX11* and a map virtually identical to the nucleosome–SOX11 from the 147-bp sample.

Extended Data Table 1 | Cryo-EM data collection, refinement and validation statistics

	Free nucleosome (EMD-10390) (PDB 6T79)	Nucleosome-SOX2 (EMD-10392) (PDB 6T7B)	Nucleosome-SOX11* (EMD-10394) (PDB 6T7D)	Nucleosome-SOX11 (EMD-10391) (PDB 6T7A)	Nucleosome-$SOX11_2$ (EMD-10393) (PDB 6T7C)
Data collection and processing					
Magnification	130 000x	130 000x	130 000x	130 000x	130 000x
Voltage (kV)	300	300	300	300	300
Electron exposure (e–/Å^2)	45	45	45	45	45
Defocus range (μm)	0.9-3.4	0.9-3.4	0.9-3.4	0.9-3.4	0.9-3.4
Pixel size (Å)	1.05	1.05	1.05	1.05	1.05
Symmetry imposed	C1	C1	C1	C1	C1
Initial particle images (no.)	451 990	2 347 743	2 521 110	4 178 143	4 178 143
Final particle images (no.)	368 270	32 301	63 821	202 142	114 104
Map resolution (Å) 0.143 FSC threshold	3.2	5.1	4.3	3.7	4.0
Map resolution range (Å)	3-3.9	4.5-8.3	4.1-6.6	3.5-5.5	3.7-5.3
Refinement					
Initial model used (PDB code)	6FQ5	6T7A	6T7A	6T79	6T7A
Model resolution (Å) FSC threshold	3.2	5.1	4.3	3.7	4.0
Model resolution range (Å)	3-3.9	4.5-8.3	4.1-6.6	3.5-5.5	3.7-5.3
Map sharpening *B* factor (Å^2)	-75	-100	-100	-100	-120
Model composition					
Non-hydrogen atoms	12121	7248	8209	10338	7558
Protein residues	776	838	853	847	916
DNA	290	190	234	190	190
B factors (Å^2)					
Protein	33	76	140	89	106
DNA	81	139	210	140	140
R.m.s. deviations					
Bond lengths (Å)	0.52	0.60	055	0.52	0.56
Bond angles (°)	0.83	0.88	0.93	0.79	0.86
Validation					
MolProbity score	1.28	1.84	2.85	1.37	0.94
Clashscore	5	1	3	7	2
Poor rotamers (%)	0	na*	na*	0	na*
Ramachandran plot					
Favored (%)	99	na*	na*	98.1	na*
Allowed (%)	1	na*	na*	1.8	na*
Disallowed (%)	0	na*	na*	0.1	na*

na*, model is deposited as backbone only (owing to insufficient resolution of the cryo-EM map).

Extended Data Table 2 | Data collection and refinement statistics (molecular replacement)

	SOX11-DNA PDB 6T78
Data collection	
Space group	P 6_1
Cell dimensions	
a, *b*, *c* (Å)	106.1, 106.1, 76.9
α, β, γ (°)	90 90 120
Wavelength (Å)	1
Resolution (Å)	46 - 2.5 (2.6-2.5)
R_{merge}	0.13 (2.8)
$I / \sigma I$	17.3 (1.28)
Completeness (%)	99.7 (98.7)
Redundancy	20.5 (20.3)
Refinement	
Resolution (Å)	2.5
No. reflections	17033 (1682)
R_{work} / R_{free}	0.23 / 0.26
No. atoms	2332
Protein	1307
DNA	1019
Water	6
B-factors	96
Protein	83
DNA	114
Water	65
R.m.s. deviations	
Bond lengths (Å)	0.01
Bond angles (°)	0.8

Number of crystals = 1. Values in parentheses are for the highest-resolution shell.

nature research

Corresponding author(s): Patrick Cramer

Last updated by author(s): Mar 6, 2020

Reporting Summary

Nature Research wishes to improve the reproducibility of the work that we publish. This form provides structure for consistency and transparency in reporting. For further information on Nature Research policies, see Authors & Referees and the Editorial Policy Checklist .

Statistics

For all statistical analyses, confirm that the following items are present in the figure legend, table legend, main text, or Methods section.

n/a	Confirmed	
☐	☒	The exact sample size (*n*) for each experimental group/condition, given as a discrete number and unit of measurement
☐	☒	A statement on whether measurements were taken from distinct samples or whether the same sample was measured repeatedly
☒	☐	The statistical test(s) used AND whether they are one- or two-sided *Only common tests should be described solely by name; describe more complex techniques in the Methods section.*
☒	☐	A description of all covariates tested
☒	☐	A description of any assumptions or corrections, such as tests of normality and adjustment for multiple comparisons
☐	☒	A full description of the statistical parameters including central tendency (e.g. means) or other basic estimates (e.g. regression coefficient) AND variation (e.g. standard deviation) or associated estimates of uncertainty (e.g. confidence intervals)
☒	☐	For null hypothesis testing, the test statistic (e.g. *F*, *t*, *r*) with confidence intervals, effect sizes, degrees of freedom and *P* value noted *Give P values as exact values whenever suitable.*
☒	☐	For Bayesian analysis, information on the choice of priors and Markov chain Monte Carlo settings
☒	☐	For hierarchical and complex designs, identification of the appropriate level for tests and full reporting of outcomes
☒	☐	Estimates of effect sizes (e.g. Cohen's *d*, Pearson's *r*), indicating how they were calculated

Our web collection on statistics for biologists contains articles on many of the points above.

Software and code

Policy information about availability of computer code

Data collection	FEI EPU 1.10;
Data analysis	Warp 1.0.6; RELION 3.0; Gautomatch v0.56, Gctf v1.06, CryoSPARC v2; COOT v. 0.8.9.1; PHENIX v. 1.14; Pymol v. 2.2.3; Chimera v. 1.13 ; Molprobity 4.5 server; 3DFSC server; ImageJ 1.52k; Microsoft Excel 14.7.7; XSCALE BUILT=20170601; PHASER 1.2;

For manuscripts utilizing custom algorithms or software that are central to the research but not yet described in published literature, software must be made available to editors/reviewers. We strongly encourage code deposition in a community repository (e.g. GitHub). See the Nature Research guidelines for submitting code & software for further information.

Data

Policy information about availability of data

All manuscripts must include a data availability statement. This statement should provide the following information, where applicable:

- Accession codes, unique identifiers, or web links for publicly available datasets
- A list of figures that have associated raw data
- A description of any restrictions on data availability

The electron density reconstructions and corresponding models were deposited with the Electron Microscopy Data Base (EMD-10390, EMD-10391, EMD-10392, EMD-10393, EMD-10394) and with the Protein Data Bank (6T78, 6T79, 6T7A, 6T7B, 6T7C, 6T7D). Source data is relevant for Fig. 2, ED Figures 2,4,5,6,10,13

Field-specific reporting

Please select the one below that is the best fit for your research. If you are not sure, read the appropriate sections before making your selection.

☒

Life sciences study design

All studies must disclose on these points even when the disclosure is negative.

Sample size	Numbers of particles used for cryo-EM reconstructions are listed in Extended Table 1. Sample sizes were estimated on the basis of previous studies using similar methods and analyses that are widely published.
Data exclusions	No data were excluded from the analysis.
Replication	All attempts at replication were successful and reproducible. At least two independent biological repeats per experiment performed and showed similar results. Structure determination does not require replication.
Randomization	Samples were not allocated into groups. Randomization is not relevant to this study.
Blinding	Blinding was not relevant to this study because there was no group allocation.

Reporting for specific materials, systems and methods

We require information from authors about some types of materials, experimental systems and methods used in many studies. Here, indicate whether each material, system or method listed is relevant to your study. If you are not sure if a list item applies to your research, read the appropriate section before selecting a response.

Materials & experimental systems

n/a	Involved in the study
☒	☐ Antibodies
☒	☐ Eukaryotic cell lines
☒	☐ Palaeontology
☒	☐ Animals and other organisms
☒	☐ Human research participants
☒	☐ Clinical data

Methods

n/a	Involved in the study
☒	☐ ChIP-seq
☒	☐ Flow cytometry
☒	☐ MRI-based neuroimaging